

Supplementary Material: Impressive Transport Properties of Be₂C Monolayer

Gautam Sharma^{1, a)} and K.C. Bhamu²

¹⁾*Department of Physics, Indian Institute of Science Education and Research Pune, Pune, India*

²⁾*PMC Division, CSIR-National Chemical Laboratory, Pune-411008, India*

^{a)}Electronic mail: gautam.iiser@gmail.com

I. TRANSPORT PROPERTIES

Transport properties are shown as a function of hole and electron doping along armchair direction for Be_2C monolayer.

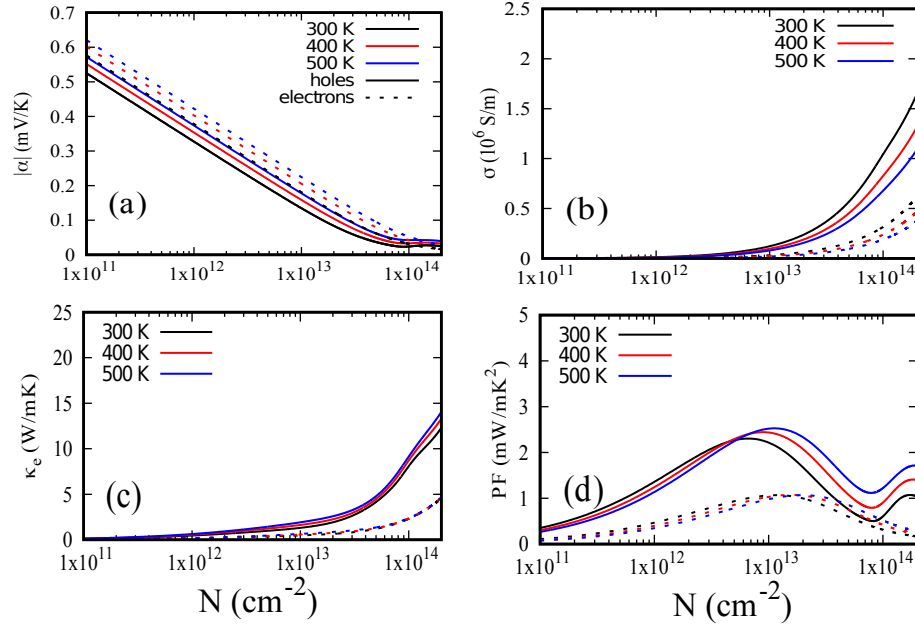


FIG. S1. The Seebeck coefficient (a) electrical conductivity (b) power factor (c) electronic thermal conductivity (d) with hole (electron) doping along armchair direction is shown by solid (dashed) lines at 300 K, 400 K and 500K represented by black, red and blue lines respectively.

Impressive Transport Properties of Be₂C Monolayer

Gautam Sharma^{1, a)} and K.C. Bhamu²

¹⁾*Department of Physics, Indian Institute of Science Education and Research Pune, Pune, India*

²⁾*PMC Division, CSIR-National Chemical Laboratory, Pune-411008, India*

We present thermoelectric properties of Be₂C monolayer based on density functional theory and semi-classical Boltzmann transport theory. Electronic structure calculations predict this material as a semiconductor with a direct bandgap of 2.0 eV computed using Gaussian-attenuating Perdew-Burke-Ernzerhof (Gau-PBE) hybrid functional. The Gau-PBE band structure is used to compute transport properties by solving the Boltzmann transport equation under the constant relaxation time approximation. In this work, we have explicitly determined the relaxation time by studying the electron-phonon interactions in the system to estimate absolute transport coefficients. Our results show that the monolayer possesses a high power factor (~ 3.44 mW/mK²), similar to the commercial TE materials doped-Bi₂Te₃ and PbTe, suggesting that Be₂C monolayer is a promising thermoelectric material.

^{a)}Electronic mail: gautam.iiser@gmail.com

I. INTRODUCTION

Increasing consumption of natural energy resources demanded the scientific community to switch their attention to sustainable energy resources. Waste heat management technology is one of the efficient and economical alternatives for power generation. Thermoelectric (TE) materials have gained tremendous attention for their ability to convert the waste heat ejected from automobiles and industries into electricity. The figure of merit, $ZT = \alpha^2 \sigma T / \kappa$, is the crucial quantity that describes a TE material's efficiency, where T , α , σ , and κ denote temperature, Seebeck coefficient, electrical conductivity, and total thermal conductivity, respectively. The total thermal conductivity is the sum of the electronic (κ_e) and lattice thermal conductivity (κ_l). ZT can be maximized by increasing the power factor (PF, $PF = \alpha^2 \sigma$) and simultaneously decreasing the thermal conductivity (κ). However, it is very challenging to achieve high PF because of the interdependence of the quantities involved. For example, if one tries to enhance σ through doping the material, it reduces α . Moreover, an increase in σ also increases κ_e as Wiedemann-Franz Law connects them. Therefore it is not easy to control these parameters independently and thus to optimize ZT of a material.

Despite these challenges, TE performance of the material can be tuned by various ways like convergence of multiple bands,¹² combination of light-heavy bands³, multivalley carrier pocket⁴ and reduced dimensionality.⁵ Dresselhaus *et al.* have shown theoretically that low-dimensional systems would attain higher ZT than their bulk counterpart⁶⁷. Recent advances to improve ZT are centered around reducing dimensionality, for instance, monolayer Bi_2Te_3 have shown high ZT than its bulk counterpart⁸⁹¹⁰. Similarly, nanostructured materials have also shown better TE performance¹¹.

In this work, we study thermoelectric properties of Be_2C monolayer (Be_2C -ML) in its global minimum energy structure using density functional theory (DFT) based calculations and semi-classical Boltzmann transport theory (BTT). Be_2C -ML is found to be a semiconductor with a bandgap of 2.34 eV computed with Heyd-Scuseria-Ernzerhof (HSE) functional¹². In a computational study, Naseri *et al.* have investigated electronic and optical properties of the Be_2C -ML under stress and strain¹³. Yeoh *et al.* have studied Be_2C -ML as the anode material for Lithium-ion battery applications¹⁴. Notably, Be and C elements are earth-abundant relative to elements (like Pb, Bi, and Te) used for commercial TE ma-

terials. Moreover, a molecular dynamics-based study has shown that the Be₂C-ML has a high melting point around 1500 K, and therefore, it has the potential to show stunning TE properties at high temperature¹².

The electronic band structure shows that it has doubly degenerate valence bands with different band curvatures around the Brillouin zone center. Such a band feature is often desirable in TE materials as it provides both light and heavy hole pockets to enhance the transport properties^{3,12}. To the best of our knowledge, TE properties of the Be₂C-ML are still waiting to uncover. These factors have motivated us to investigate the TE properties of the Be₂C-ML, which includes studying the electron-phonon interactions (EPIs) and thereby calculating the relaxation time of charge carriers in the system. The rest of the manuscript is organized as follows. Section II provides the details of computational methods used to investigate various properties. Section III discusses electronic structure, EPIs and TE properties of the Be₂C-ML. Conclusive remarks are presented in Section IV.

II. COMPUTATIONAL DETAILS

A. DFT calculations

First-principles calculations are performed with the Quantum ESPRESSO software, which is a plane-wave based implementation of density functional theory (DFT)^{15,16}. The electronic exchange-correlation potential is described by the generalized gradient approximation (GGA) as parametrized by Perdew, Burke, and Ernzerhof (PBE)¹⁷. We have used the norm-conserving Trouiller-Martins pseudopotentials to describe the electron-ion interactions¹⁸. These pseudopotentials have been generated using 2s² 2p⁰ 3d⁰ 4f⁰ and 2s² 2p² 3d⁰ 4f⁰ valence configurations for Be and C, respectively. The wave functions are expanded in a plane wave basis, defined by the kinetic energy cut-off of 85 Ry. Brillouin zone (BZ) integrations are performed using a Monkhorst-Pack k -point grid of (11×11×1) for the monolayer¹⁹. We have included semi-empirical Grimme-D2 van der Waals (vdW) corrections in all the calculations²⁰. For a better estimate of the bandgap, we have performed hybrid calculations using the singularity free Gaussian-attenuating Perdew-Burke-Ernzerhof (Gau-PBE) functional²¹. The matrix elements of the Fock operator are evaluated with a (5×5×1) q -grid for the ML. We have used a vacuum of length L , 15 Å, to eliminate the

spurious interactions due to periodic images present along the z-axis.

B. Relaxation time (τ) calculations:

Within Migdal approximation, the electron self-energy ($\Sigma_{n,k} = \Sigma'_{n,k} + i\Sigma''_{n,k}$) is given by^{22,23}

$$\Sigma_{n,k} = \sum_{q\nu,m} w_q |g_{q\nu,m}(k, q)|^2 \left[\frac{n_{q\nu} + 1 - f_{mk+q}}{\epsilon_{nk} - \epsilon_{mk+q} - \hbar\omega_{q\nu} - i\delta} + \frac{n_{q\nu} + f_{mk+q}}{\epsilon_{nk} - \epsilon_{mk+q} + \hbar\omega_{q\nu} - i\delta} \right] \quad (1)$$

where $g_{q\nu,m}$ is electron-phonon (el-ph) matrix element. $n_{q\nu}$ and f_{mk} are the Bose and Fermi occupation factors respectively. $\omega_{q\nu}$ is the phonon frequency for mode ν and wavevector q and ϵ_{nk} are the Kohn-Sham eigenvalues for band n and wavevector k . The imaginary part of self-energy of the electron ($\text{Im}\Sigma_{n,k}$) is computed with the EPW package²⁴. The $\text{Im}\Sigma_{n,k}$ is related to the relaxation time as follows:

$$\tau_{n,k} = \frac{\hbar}{2\text{Im}\Sigma_{n,k}} \quad (2)$$

where \hbar is the reduced Planck's constant. We calculate the electron self-energy using PBE functional, firstly, we compute el-ph matrix elements (g_{mn}^ν) on a coarse ($18 \times 18 \times 1$) k -grid and ($9 \times 9 \times 1$) q -grid. To obtain converged results, the coarse k and q -grids are interpolated on a ($25 \times 25 \times 1$) k -grid and a dense ($280 \times 280 \times 1$) q -grid respectively.

C. Boltzmann transport calculations:

Transport coefficients such as Seebeck coefficient (α), electrical conductivity (σ) can be calculated using semi-classical Boltzmann Transport equation (BTE)²⁵. BoltzTraP package is used to solve the BTE to provide TE coefficients within the rigid band approximation (RBA) and constant relaxation time approximations (CRTA)²⁶. Within RBA, doping and temperature effects on the band energies are ignored. The chemical potential (μ) is shifted above/below for electron/hole doping. We have found the convergence in transport coefficients computed based on the electronic structure calculations performed with Gau-PBE functional using a dense ($35 \times 35 \times 1$) k -grid.

III. RESULTS AND DISCUSSIONS

A. Crystal structure

Be_2C exists in the hexagonal crystal structure with space group $P-3m1$ (Fig. 1). The Be_2C -ML is made of three atomic sublayers with C atoms sandwiched by two Be-layers stacked along the z-direction. Within Be_2C -ML, each C atom is connected with six Be atoms, and each Be atom is connected with three C, and three Be atoms. The optimized Be-C and Be-Be bond lengths are 1.76 Å and 1.93 Å, respectively. These values agree well with the previous report¹². The intralayer distance between the two Be layers is $\Delta \sim 0.91$ Å and that between the C and the Be layer is ~ 0.45 Å as acquired from the present study. Our calculations with PBE functional yield lattice parameter, $a = 2.95$ Å, and it is in excellent agreement with the previously reported value 2.99 Å¹².

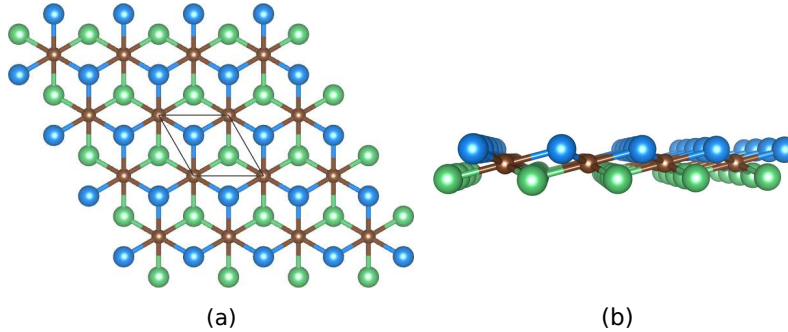


FIG. 1. (a) Top and (b) side view of the Be_2C -ML. Beryllium atoms are represented by dark blue (top) and light green (bottom) spheres and the carbon atoms in the middle layer are represented by brown spheres.

B. Electronic band structure and density of states

The PBE band structure of Be_2C -ML (red solid lines) with vdW corrections is shown in Fig. 2 (a). We observe a direct bandgap of 1.62 eV with the valence band maxima (VBM) and the conduction band minima (CBM) located at Γ point of BZ. Since PBE functional underestimates the bandgap, we calculate the band structure with Gau-PBE hybrid functionals with vdW corrections to predict the accurate bandgap. These functionals provide Kohn-Sham eigenvalues as accurate as can be obtained by HSE hybrid functionals

with very less computational cost²¹. We find that Gau-PBE predicts the bandgap of 2.0 eV, whereas the band dispersion remains intact compared to PBE as shown in Fig. 2 (a) (solid green lines). The computed band gap is 0.34 eV lower than that previously reported with HSE¹². The total density of states (DOS) and those projected onto the Be- s, p, d and C- p, d atomic orbitals are shown in Fig. 2 (b). We see the valence band is primarily composed of the C- p states, while the conduction band is derived from the Be- s, d .

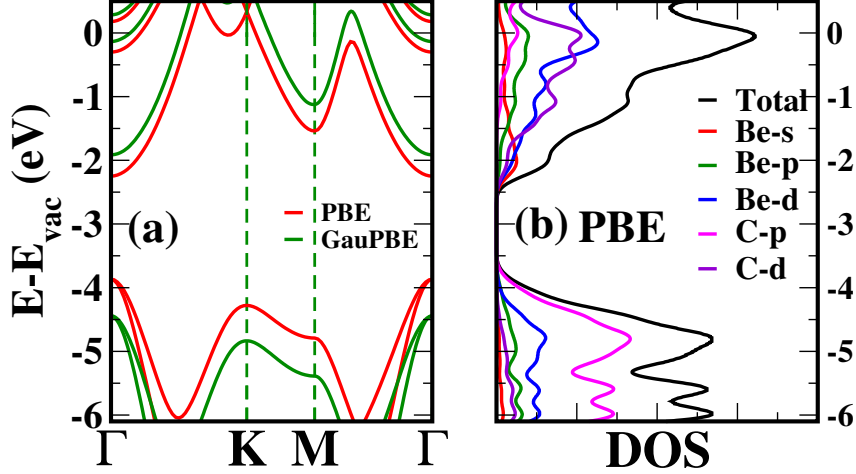


FIG. 2. (a) Band structure for Be₂C-ML with PBE (red) and Gau-PBE (green) functionals. (b) Projected density of states (PDOS) with PBE (b). The vacuum energy is chosen as zero to shift the Kohn-Sham energy eigenvalues.

C. Electron-Phonon relaxation time (τ)

The transport coefficients are produced in terms of relaxation time (τ), namely, electrical (σ/τ) and electronic thermal conductivity (κ_e/τ) when computed within Boltzmann transport framework under CRTA. Therefore, it is of prime importance to calculate τ of the charge carriers explicitly to evaluate the absolute transport coefficients. Hence we exploit the most advanced method, EPW, based on the EPIs where acoustic and optical vibrational modes are taken to be scattering channels for the charge carriers. As a result, it precisely provides information of τ compared to traditionally used deformed potential theory wherein scattering only from acoustic modes is considered, and as a result, it severely overestimates the TE coefficients^{10,27–29}. Fig. 3 (a) shows the variation of the imaginary part of self-energy for the bottom-most conduction (solid lines) and the topmost valence bands (dashed lines)

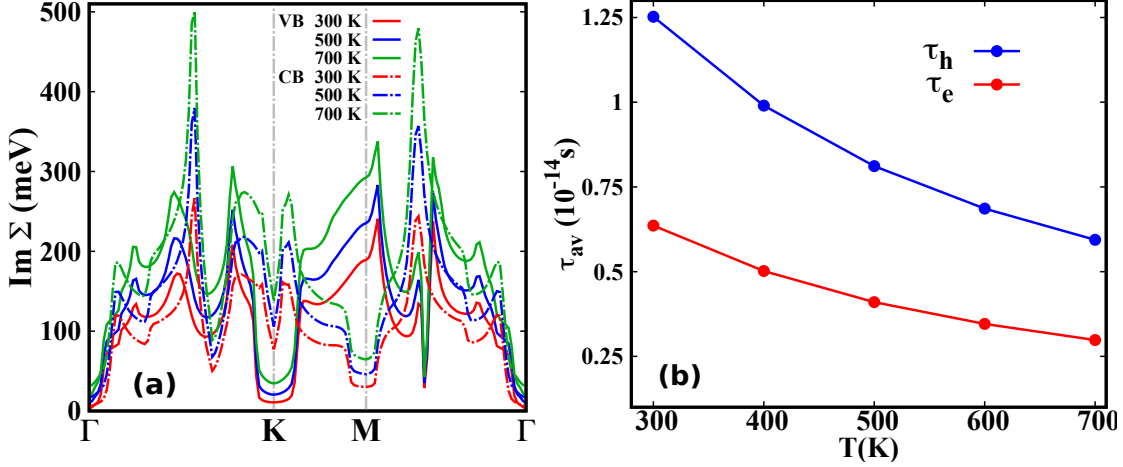


FIG. 3. (a) The variation of the imaginary part of the self-energy for the valence (Σ_{VB}) and the conduction bands (Σ_{CB}) (solid and dashed lines respectively) along the high symmetry directions in the BZ at 300K, 500K and 700K (red, blue and green respectively) for the Be_2C -ML. (b) Temperature-dependent average relaxation time (τ_{av}) for electron (red) and holes (blue).

along the high symmetry directions in the BZ for the temperatures: 300K, 500K, and 700K at Fermi energy. We find that it increases with increased temperature due to increased scattering between excited phonons and electrons. As a result, it leads to a decrease in τ_{av} with temperature, as shown in Fig. 3 (b). Here τ_{av} is obtained for a given band using $(\tau_n = \sum_k \frac{\epsilon_{n,k} \tau_{n,k}}{\epsilon_{n,k}})^{30}$. Similarly, τ_{av} can also be obtained along the zigzag and armchair directions by supplying path along the M-K and Γ -M directions in BZ, respectively. Having the information of the τ_{av} for holes/electrons at various temperatures, we compute the transport properties of the Be_2C -ML as explained in the following section.

D. Transport properties

Transport coefficients of Be_2C -ML are produced as a function of electron/hole doping at three different temperature values. Notice that we compute TE properties, namely, electrical conductivity (σ) and electronic thermal conductivity (κ_e) in the zigzag and armchair directions by incorporating τ_{av} computed in respective directions as mentioned in the previous section. Since the Seebeck coefficient (α) is obtained independent of τ within Boltzmann transport framework under CRTA. Therefore, it is expected to be the same in the two directions. Below, we discuss the transport properties along the zigzag direction and the same

along the armchair direction discussed in Supplementary Material.

In Fig. 4 (a), we plot the magnitude of the Seebeck coefficient ($|\alpha|$) as a function of carrier concentration at different temperatures for holes (solid lines) and electron doping (dashed lines). We find that the α decreases as the carrier concentration increases, and it increases with an increase in temperature, which is typical behavior of α ³¹. The value of α (at optimum PF obtained with hole doping) is found to be 0.167 mV/K with hole doping of $\sim 6.6 \times 10^{12} \text{ cm}^{-2}$ at 300 K and it is of the similar order as observed for doped-Bi₂Te₃^{32,33}. Notice that the α is greater for electrons than holes due to differences in effective masses of the carriers. The value of α for the electron doping is -0.167 mV/K at the carrier concentration of $1.2 \times 10^{13} \text{ cm}^{-2}$ at 300 K where the PF tends to optimum value with electron doping.

Fig. 4 (b) depicts the electrical conductivity for the Be₂C-ML with hole (electron) doping. The σ decreases with increased temperature since relaxation time decreases with temperature for holes and electrons. We have obtained the value of σ (at optimum PF) to be $1.22 \times 10^5 \text{ S/m}$ with hole doping of $6.6 \times 10^{12} \text{ cm}^{-2}$ at 300 K. Fig. 4 (c) presents electronic contribution to thermal conductivity with hole/electron doping. We find that κ_e is directly proportional to electrical conductivity, which is a typical trend as suggested by Wiedemann-Franz law.

Fig. 4 (d) shows the PF for the monolayer when it is hole/electron doped. The power factor is a function of α and σ where both show opposite trends when the monolayer is doped. Therefore, one is expected to find the optimum value of PF as a function of carrier concentration. For hole doped of $6.6 \times 10^{12} \text{ cm}^{-2}$, we have obtained the optimum value of PF to be $\sim 3.44 \text{ mW/mK}^2$ at 300 K which is of the same order observed for doped-Bi₂Te₃ and PbTe³²⁻³⁴. Furthermore, it increases with temperature as α ramps up with temperature. The value of optimum PF is 0.92 mW/mK^2 at the electron doping of $1.2 \times 10^{13} \text{ cm}^{-2}$, and it is almost four times lower compared to PF obtained for hole doping due to the lower electrical conductivity of the electrons.

Interestingly, the high values of PF found in our case could challenge Bi₂Te₃ and PbTe³²⁻³⁴. A similar feature has also been observed in Heusler alloy like Fe₂VAI³⁵. So our results can motivate further theoretical and experimental investigation on this material.

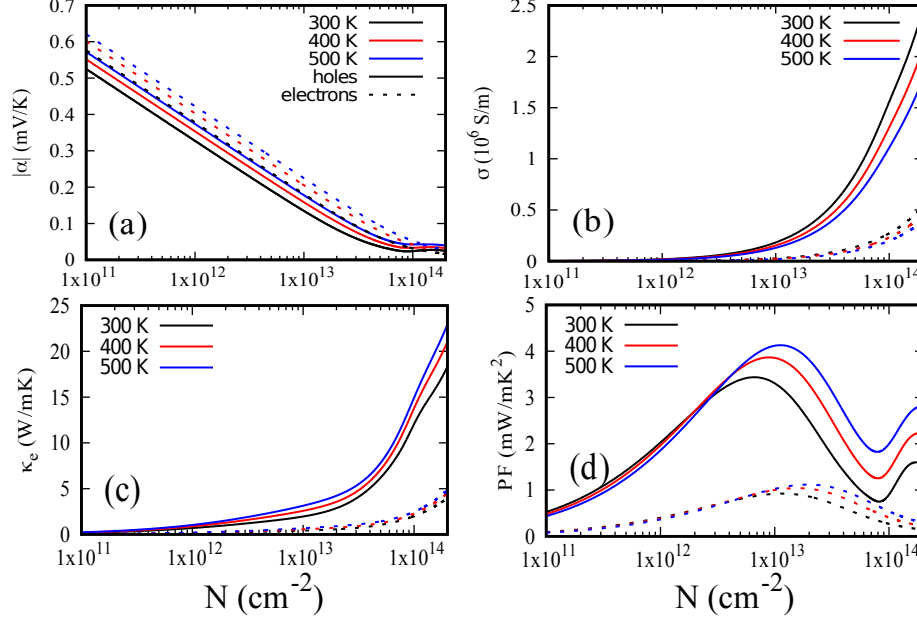


FIG. 4. The Seebeck coefficient (a) electrical conductivity (b) electronic thermal conductivity (c) power factor (d) with hole (electron) doping along the zigzag direction is shown by solid (dashed) lines at 300 K, 400 K and 500K represented by black, red and blue lines respectively.

IV. CONCLUSION

In conclusion, we have computed the electronic and transport properties of Be_2C monolayer with Gau-PBE hybrid functional. Band structure calculations show that Be_2C -ML is a direct bandgap ($E_g=2.0$ eV) material with a doubly degenerate energy band at Γ in the valence band. We have investigated electron-phonon interactions in the system to calculate the average relaxation time for charge carriers which is then incorporated in TE coefficients. The obtained value of PF (~ 3.44 mW/mK² at 300 K) is found to be of a similar order of PF as reported for many well-known TE materials like doped- Bi_2Te_3 and PbTe . Such a high value of PF reflects that Be_2C -ML may be a potential room temperature TE material.

V. SUPPLEMENTAL MATERIAL

Transport properties along armchair direction can be found in Supplementary Material.

ACKNOWLEDGMENTS

GS would like to thank IISER-Pune for the fellowship. KCB acknowledges the DST-SERB for the SERB-National Postdoctoral Fellowship (Award No. PDF/2017/002876). The research used resources at the National Energy Research Scientific Computing Center (NERSC), which is supported by the Office of Science of the U.S. DOE under Contract No. DE-AC02-05CH11231 and high performance computing Center of Development of Advanced Computing, Pune, India.

REFERENCES

- ¹M. Mukherjee, G. Yumnam, and A. K. Singh, “High thermoelectric figure of merit via tunable valley convergence coupled low thermal conductivity in Bi_2Te_3 chalcopyrites,” *The Journal of Physical Chemistry C* **122**, 29150–29157 (2018).
- ²Y. Pei, X. Shi, A. LaLonde, H. Wang, L. Chen, and G. J. Snyder, “Convergence of electronic bands for high performance bulk thermoelectrics,” *Nature* **473**, 66–69 (2011).
- ³A. F. May, D. J. Singh, and G. J. Snyder, “Influence of band structure on the large thermoelectric performance of lanthanum telluride,” *Phys. Rev. B* **79**, 153101 (2009).
- ⁴H. J. Goldsmid, *Thermoelectric Refrigeration* (Plenum, New York, 1964).
- ⁵D. Parker, X. Chen, and D. J. Singh, “High three-dimensional thermoelectric performance from low-dimensional bands,” *Phys. Rev. Lett.* **110**, 146601 (2013).
- ⁶L. D. Hicks and M. S. Dresselhaus, “Effect of quantum-well structures on the thermoelectric figure of merit,” *Phys. Rev. B* **47**, 12727–12731 (1993).
- ⁷L. D. Hicks and M. S. Dresselhaus, “Thermoelectric figure of merit of a one-dimensional conductor,” *Phys. Rev. B* **47**, 16631–16634 (1993).
- ⁸S. Sharma and U. Schwingenschlög, “Thermoelectric response in single quintuple layer Bi_2Te_3 ,” *ACS Energy Letters* **1**, 875–879 (2016).
- ⁹J. S. Son, M. K. Choi, M.-K. Han, K. Park, J.-Y. Kim, S. J. Lim, M. Oh, Y. Kuk, C. Park, S.-J. Kim, and T. Hyeon, “n-type nanostructured thermoelectric materials prepared from chemically synthesized ultrathin Bi_2Te_3 nanoplates,” *Nano Letters* **12**, 640–647 (2012), pMID: 22268842.

- ¹⁰R. Fei, A. Faghaninia, R. Soklaski, J.-A. Yan, C. Lo, and L. Yang, “Enhanced thermoelectric efficiency via orthogonal electrical and thermal conductances in phosphorene,” *Nano Letters* **14**, 6393–6399 (2014), pMID: 25254626.
- ¹¹Z. L.-D. Li Jing-Feng, Liu Wei-Shu and Z. Min, “High-performance nanostructured thermoelectric materials,” *NPG Asia Materials* **2**, 152–158 (2010).
- ¹²Y. Li, Y. Liao, and Z. Chen, “Be₂C monolayer with quasi-planar hexacoordinate carbons: A global minimum structure,” *Angewandte Chemie International Edition* **53**, 7248–7252 (2014).
- ¹³M. Naseri and J. Jalilian, “Electronic and optical investigations of be₂c monolayer: Under stress and strain conditions,” *Materials Research Bulletin* **88**, 49–55 (2017).
- ¹⁴K. H. Yeoh, K.-H. Chew, Y. Z. Chu, T. L. Yoon, Rusi, and D. S. Ong, “First-principles study of monolayer be₂c as an anode material for lithium-ion batteries,” *Journal of Applied Physics* **126**, 125302 (2019).
- ¹⁵P. Giannozzi, S. Baroni, N. Bonini, M. Calandra, R. Car, C. Cavazzoni, D. Ceresoli, G. L. Chiarotti, M. Cococcioni, I. Dabo, A. Dal Corso, S. de Gironcoli, S. Fabris, G. Fratesi, R. Gebauer, U. Gerstmann, C. Gougoussis, A. Kokalj, M. Lazzeri, L. Martin-Samos, N. Marzari, F. Mauri, R. Mazzarello, S. Paolini, A. Pasquarello, L. Paulatto, C. Sbraccia, S. Scandolo, G. Schlauser, A. P. Seitsonen, A. Smogunov, P. Umari, and R. M. Wentzcovitch, “Quantum espresso: a modular and open-source software project for quantum simulations of materials,” *Journal of Physics: Condensed Matter* **21**, 395502 (19pp) (2009).
- ¹⁶P. Giannozzi, O. Andreussi, T. Brumme, O. Bunau, M. B. Nardelli, M. Calandra, R. Car, C. Cavazzoni, D. Ceresoli, M. Cococcioni, N. Colonna, I. Carnimeo, A. D. Corso, S. de Gironcoli, P. Delugas, R. A. D. Jr, A. Ferretti, A. Floris, G. Fratesi, G. Fugallo, R. Gebauer, U. Gerstmann, F. Giustino, T. Gorni, J. Jia, M. Kawamura, H.-Y. Ko, A. Kokalj, E. Küçükbenli, M. Lazzeri, M. Marsili, N. Marzari, F. Mauri, N. L. Nguyen, H.-V. Nguyen, A. O. de-la Roza, L. Paulatto, S. Poncé, D. Rocca, R. Sabatini, B. Santra, M. Schlipf, A. P. Seitsonen, A. Smogunov, I. Timrov, T. Thonhauser, P. Umari, N. Vast, X. Wu, and S. Baroni, “Advanced capabilities for materials modelling with quantum espresso,” *Journal of Physics: Condensed Matter* **29**, 465901 (2017).
- ¹⁷J. P. Perdew, K. Burke, and M. Ernzerhof, “Generalized gradient approximation made simple,” *Phys. Rev. Lett.* **77**, 3865–3868 (1996).

- ¹⁸D. R. Hamann, M. Schlüter, and C. Chiang, “Norm-conserving pseudopotentials,” *Phys. Rev. Lett.* **43**, 1494–1497 (1979).
- ¹⁹H. J. Monkhorst and J. D. Pack, “Special points for brillouin-zone integrations,” *Phys. Rev. B* **13**, 5188–5192 (1976).
- ²⁰G. Stefan, “Semiempirical gga-type density functional constructed with a long-range dispersion correction,” *Journal of Computational Chemistry* **27**, 1787–1799 (2006).
- ²¹J.-W. Song, G. Giorgi, K. Yamashita, and K. Hirao, “Communication: Singularity-free hybrid functional with a gaussian-attenuating exact exchange in a plane-wave basis,” *The Journal of Chemical Physics* **138**, 241101 (2013), <https://doi.org/10.1063/1.4811775>.
- ²²A. Migdal, “Interactions between electrons and lattice vibrations in a normal metal,” *Zhur. Eksp. Teor. Fiz.* **34** (1958).
- ²³G. Eliashberg, “Interactions between electrons and lattice vibrations in a superconductor,” *Sov. Phys. JETP* **7** (1960).
- ²⁴S. Poncé, E. Margine, C. Verdi, and F. Giustino, “Epw: Electron-phonon coupling, transport and superconducting properties using maximally localized wannier functions,” *Computer Physics Communications* **209**, 116–133 (2016).
- ²⁵G. D. Mahan and J. O. Sofo, “The best thermoelectric,” *Proceedings of the National Academy of Sciences* **93**, 7436–7439 (1996), <https://www.pnas.org/content/93/15/7436.full.pdf>.
- ²⁶G. K. Madsen and D. J. Singh, “Boltztrap. a code for calculating band-structure dependent quantities,” *Computer Physics Communications* **175**, 67 – 71 (2006).
- ²⁷B. Liao, J. Zhou, B. Qiu, M. S. Dresselhaus, and G. Chen, “Ab initio study of electron-phonon interaction in phosphorene,” *Phys. Rev. B* **91**, 235419 (2015).
- ²⁸Y. Nakamura, T. Zhao, J. Xi, W. Shi, D. Wang, and Z. Shuai, “Intrinsic charge transport in stanene: Roles of bucklings and electron-phonon couplings,” *Advanced Electronic Materials* **3**, 1700143 (2017), <https://www.onlinelibrary.wiley.com/doi/pdf/10.1002/aelm.201700143>.
- ²⁹G. Sharma, V. K. Pandey, S. Datta, and P. Ghosh, “Effect of electron–phonon coupling on the transport properties of monolayers of zrs2, bii3 and pbi2: a thermoelectric perspective,” *Phys. Chem. Chem. Phys.* **23**, 11663–11671 (2021).

- ³⁰N. T. Hung, A. R. T. Nugraha, and R. Saito, “Universal curve of optimum thermoelectric figures of merit for bulk and low-dimensional semiconductors,” *Phys. Rev. Applied* **9**, 024019 (2018).
- ³¹Snyder, G. Jeffrey and Toberer, Eric S., “Complex thermoelectric materials,” *Nature Materials* **7**, 105–114 (2008).
- ³²O. Yamashita, S. Tomiyoshi, and K. Makita, “Bismuth telluride compounds with high thermoelectric figures of merit,” *Journal of Applied Physics* **93**, 368–374 (2003).
- ³³S. V. Ovsyannikov, V. V. Shchennikov, G. V. Vorontsov, A. Y. Manakov, A. Y. Likhacheva, and V. A. Kulbachinskii, “Giant improvement of thermoelectric power factor of Bi_2Te_3 under pressure,” *Journal of Applied Physics* **104**, 053713 (2008).
- ³⁴B. Paul, P. K. Rawat, and P. Banerji, “Dramatic enhancement of thermoelectric power factor in PbTe:Cr co-doped with iodine,” *Applied Physics Letters* **98**, 262101 (2011), <https://doi.org/10.1063/1.3603962>.
- ³⁵E. Alleno, “Review of the thermoelectric properties in nanostructured Fe_2VAl ,” *Metals* **8** (2018).